ACS APPLIED NANO MATERIALS

www.acsanm.org Letter

Direct Observation of Charge Transfer between NO_x and Monolayer MoS_2 by Operando Scanning Photoelectron Microscopy

Ingvild J. T. Jensen, Ayaz Ali, Patrick Zeller, Matteo Amati, Matthias Schrade, Per Erik Vullum, Marta Benthem Muñiz, Prashant Bisht, Takashi Taniguchi, Kenji Watanabe, Bodh Raj Mehta, Luca Gregoratti,* and Branson D. Belle*

Cite This: *ACS Appl. Nano Mater.* 2021, 4, 3319−3324 Read Online

ACCESS | Metrics & More | Article Recommendations | Supporting Information

ABSTRACT: Atomically thin transition-metal dichalcogenides (MoS_2, WSe_2, etc.) have long been touted as promising materials for gas detection because of their tunable band gaps; however, the sensing mechanism, based on a charge-transfer process, has not been fully explored. Here, we directly observe the effect of this charge transfer on the doping levels in MoS_2 upon exposure to NO_x by performing scanning photoelectron microscopy (SPEM) on a monolayer MoS_2 transistor under bias conditions in a gas environment. By a comparison of the operando SPEM maps of the transistor with and without exposure to NO_x gas, a downward shift in the Fermi level position could be detected, consistent with NO_x gas making the MoS_2 channel less n-type.

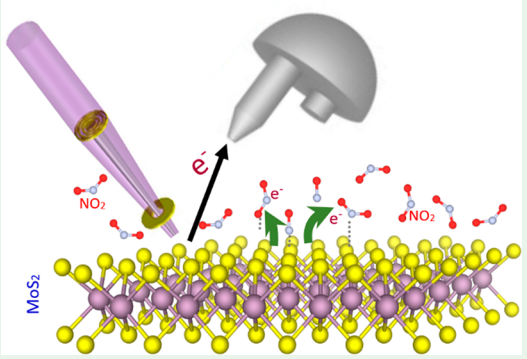

KEYWORDS: *molybdenum disulfide (MoS_2), in situ, field-effect transistor (FET), gas sensor, scanning photoelectron microscopy (SPEM), X-ray photoelectron microscopy (XPS), NO_x*

Global urbanization and industrialization have led to significant increases in the levels of air pollutants.[1] These air pollutants, such as NO and NO_2, are detrimental to human health and must therefore be closely monitored.[2] Currently, gas sensors based on metal oxide films are the predominant technology used in environmental monitoring systems. They do, however, require elevated temperatures and exhibit sensitivities limited to the low parts per million range.[3] Two-dimensional (2D)-layered nanomaterials and their heterostructures have shown promising results in the development of ultrasensitive gas sensors because of their high surface-to-volume ratios, high carrier mobilities, and tunable band gaps.[4] Graphene-based gas sensors have even shown single-gas-molecule detection at room temperature.[5] Among the various 2D-layered nanomaterials, molybdenum disulfide (MoS_2) has been widely used in gas sensor research because of its layer-dependent tunable band gap (2.8−1.9 eV),[6] wafer-scale fabrication[7] with various active sites (sulfur defects, vacancy defects, and edge sites), and relatively high mobilities.[8] Sensitivities down to parts per billion toward NO and NO_2 have been demonstrated,[4,9] which makes it clear that MoS_2 field-effect transistors (FETs) can be used as highly sensitive gas sensors.

The sensing mechanism of n-type MoS_2 is believed to be based on a charge-transfer process,[10,11] where oxidizing and reducing gases accept or donate electrons from the channel during adsorption, thereby increasing or reducing the resistance, respectively. To validate the charge-transfer mechanism in the presence of a gas environment, various techniques have been used, such as Kelvin probe force microscopy,[12] in situ Raman spectroscopy,[13] photoluminescence,[11] and ultraviolet photoemission spectroscopy.[14] Notwithstanding, experiments that directly probe the interaction between the gas and MoS_2 at the interface are still lacking.

Here, for the first time, the electrical and chemical interactions between gas molecules and monolayer MoS_2 are probed simultaneously by employing scanning photoelectron microscopy (SPEM) at the Elettra synchrotron's ESCA microscopy beamline.[15,16] By performing spatially resolved operando photoelectron spectroscopy on a monolayer MoS_2 transistor under different bias conditions in a gas environment, we demonstrate that charge transfer is the main sensing mechanism of MoS_2 toward NO_x.

MoS_2/hexagonal boron nitride (hBN) FETs, as illustrated in Figure 1a, were fabricated on highly doped oxidized (300 nm) silicon wafers using a dry transfer technique,[17] followed by

Received: January 15, 2021
Accepted: February 24, 2021
Published: March 2, 2021

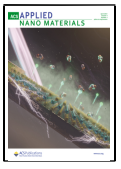

https://dx.doi.org/10.1021/acsanm.1c00137
ACS Appl. Nano Mater. 2021, 4, 3319−3324

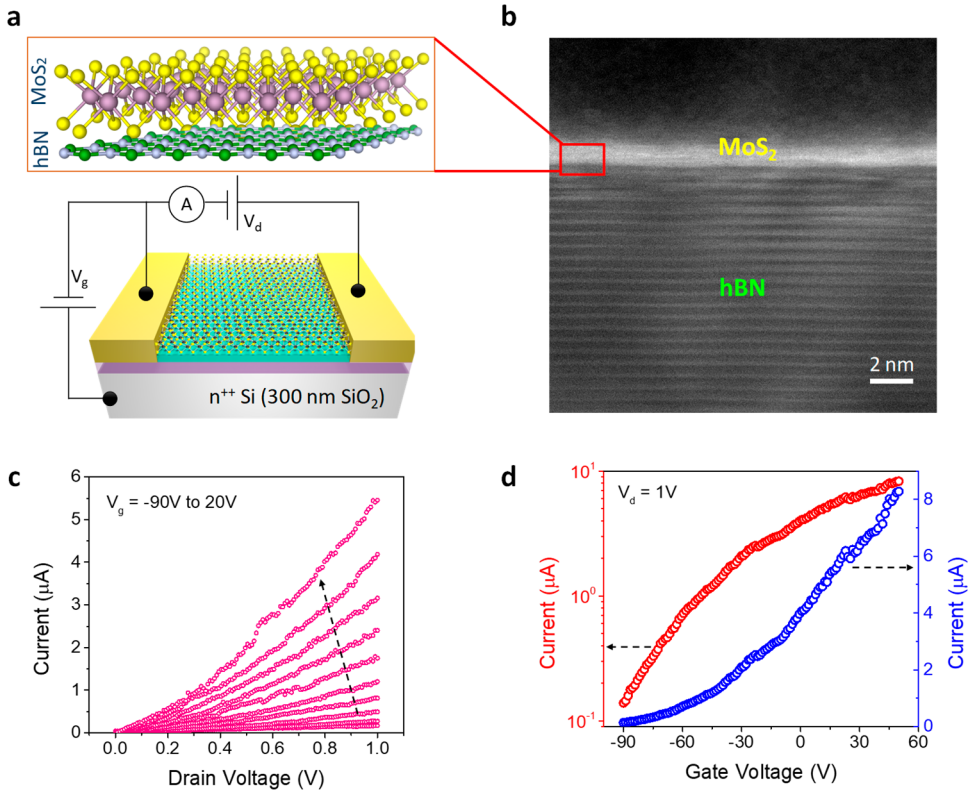

Figure 1. (a) Device schematic of a monolayer MoS_2/hBN transistor. (b) Cross-sectional LAADF STEM image of the MoS_2/hBN heterostructure. (c) Output characteristics (V_d–I_d) curves at different gate voltages (V_g = −90 to +20 V). (d) Transfer characteristics (V_g–I_d) at a drain voltage (V_d) of 1 V shown in linear (blue curve) and logarithmic (red curve) scale.

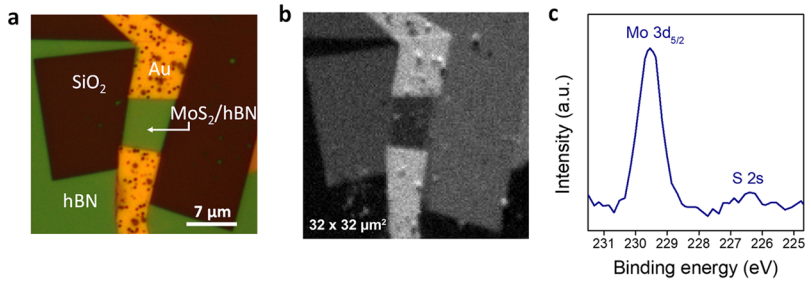

Figure 2. (a) Optical image of a MoS_2/hBN device. (b) Corresponding SPEM map of the same device acquired at the Mo $3d_{5/2}$/S 2s signal at a BE of 228.3 eV, with contacts grounded and in UHV. (c) Averaged Mo 3d spectrum extracted from the MoS_2 channel area in the SPEM map shown in part b.

standard electron-beam lithography (EBL), the details of which are given in Figure S1. The interface of the MoS_2/hBN heterojunction was characterized by cross-sectional high-resolution low-angle annular dark field scanning transmission electron microscopy (LAADF STEM), as shown in Figure 1b, confirming that our devices are indeed monolayer with clean interfaces. The devices were annealed in ultrahigh vacuum (UHV) at 300 °C for several hours prior to measurements to desorb adsorbates from the fabrication process. Figure 1c shows typical current (I)–voltage (V) curves between the source and drain. The observed nonlinearity of the I–V curves indicate a non-ohmic, slightly rectifying character of the metallic contacts, also visible in our SPEM maps discussed later. The transfer curves shown in Figure 1d demonstrate that the device is n-type with a mobility of 4 $cm^2\ V^{-1}\ s^{-1}$.

The FETs were mounted onto the SPEM with three independent electrical contacts for gate (V_g), source (V_s), and drain (V_d). SPEM maps were acquired to characterize the device in different states of operation. Figure 2a shows an optical image of one such device, while Figure 2b shows the corresponding SPEM map acquired at the Mo $3d_{5/2}$/S 2s signal, showing excellent agreement. The intensity of the MoS_2 channel is not the brightest in the maps shown in Figures 2b and S5a–d because the grayscale is based on the total intensity in the acquired spectrum. An increase in the background caused by strong peaks at lower binding energy (BE), e.g., from Au 4f, will make the pixel appear bright. Each pixel of the SPEM map contains an X-ray photoelectron spectroscopy (XPS) spectrum and shows the integral intensity of the spectrum (see the experimental section for details). Figure 2c shows an extracted spectrum averaged over the area of the MoS_2 channel.

A mixture of argon and NO_x (1.7 ppm of NO and 1.9 ppm of NO_2) was dosed into the chamber at a total pressure of 4.1

https://dx.doi.org/10.1021/acsanm.1c00137
ACS Appl. Nano Mater. 2021, 4, 3319–3324

× 10^{-6} mbar, while operando XPS and electrical data were measured. Figure 3 shows the device response to NO_x for the

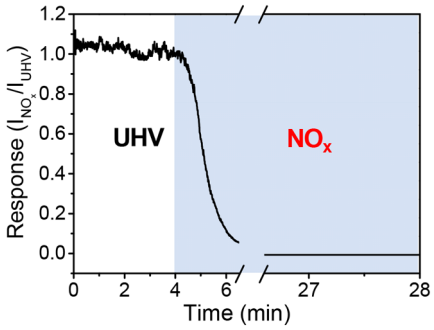

Figure 3. Electrical response to NO_x measured in situ just before the operando measurements.

device shown in Figure 4a. The current in the device decreases upon exposure to NO_x, which is expected given the oxidizing nature of the gas, and equilibrates below the instrumental resolution of the sourcemeter (10 nA) within a few minutes.

This fast decrease in the current is remarkable given the low partial pressure of NO_x of ~10^{-11} mbar inside the chamber. We rationalize this observation as the combined effect of two processes with different time constants, as had been observed earlier for NO_x adsorption on MoS_2:[13,18] (i) a rapid decrease of the carrier mobility (cf. Figure S3) and (ii) a slower decrease of the charge-carrier concentration due to charge transfer between adsorbed gas species and MoS_2. When these two effects are combined, the experimental response curve can be quantitatively described (Figure S4).

The low pressure in the chamber raises questions regarding the type of interaction between MoS_2 and adsorbed NO_x molecules. For comparison, physiosorbed O_2 is only weakly bound to MoS_2 and can be removed by exposing the sample to mild vacuum pressures of 10^{-3} mbar.[19] In contrast, for recovery after NO_x exposure, MoS_2 samples need to be annealed or illuminated,[20] indicating a much stronger binding. Indeed, the BE for physiosorbed NO_2 is significantly higher than that for O_2.[21] Moreover, oxidizing gas species can bind strongly to the surface of MoS_2 in the vicinity of sulfur vacancies by forming chemical bonds.[22]

Operando high-resolution SPEM maps of the same sample area (Figure 4a) with and without NO_x gas in the analysis chamber are presented in Figure 4b,c. In both cases, V_d was set to 1 V, and the two maps correspond to the device operated in the two steady states of the response curve in Figure 3. The maps in Figure 4b,c show the position of the Mo $3d_{5/2}$ peak maximum, which was obtained by peak fitting each spectrum (see the experimental section for details). The local BE of the core levels is a direct probe of the potential distribution of electrons between the source and drain. The maps in Figure 4b,c show shifts in the Mo 3d peak position along the channel, from 230.3 eV at the source contact at the top (located just outside the frame of the maps) to 229.3 eV at the drain contact at the bottom, within the range set by the applied V_d = 1 V. Most of the potential drop is known to occur in the regions close to the metallic contacts.[23]

Spatial inhomogeneity in the direction perpendicular to the applied bias can be observed in the maps. In the region close to the source contact, the lateral injection region formed by the Schottky contact between Ti/Au and MoS_2 is easily observed as a blue V-shaped region of high BE peak positions.[24] Small-scale inhomogeneities in the channel could be the result of trapped impurities. Although our dry transfer process in the assembly of MoS_2/hBN stacks results in clean interfaces, as demonstrated in Figure 1b, it is well-known that pockets of

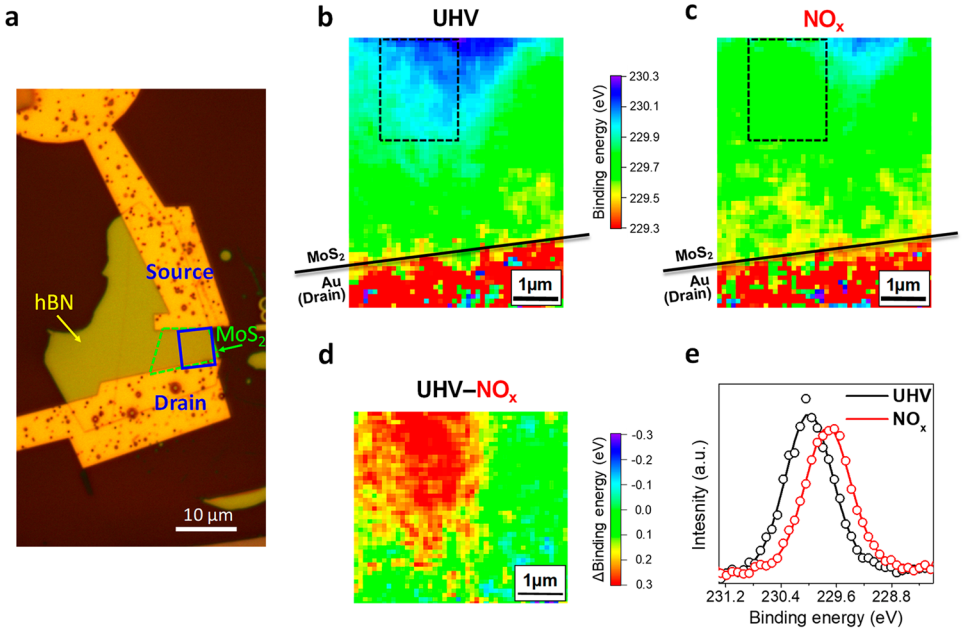

Figure 4. (a) Optical microscopy image of a single-layer MoS_2/hBN device. The blue square indicates the area investigated by SPEM. Operando SPEM maps from the Mo $3d_{5/2}$/S 2s energy region of the same MoS_2/hBN device acquired in UHV (b) and in NO_x (c), with an applied bias V_d = 1 V. The color refers to the Mo $3d_{5/2}$ BE position. The grounded gold contact is seen in red at the bottom of the maps, while the positive contact is located slightly above the top of the image not in view. (d) Difference between the Mo $3d_{5/2}$ peak position in UHV and NO_x. (e) Extracted Mo $3d_{5/2}$ spectra averaged over the area indicated by the dark dotted box in parts b and c.

https://dx.doi.org/10.1021/acsanm.1c00137
ACS Appl. Nano Mater. 2021, 4, 3319−3324

hydrocarbons and water can become trapped between the individual layers during the transfer process. These pockets of contamination could create small areas of strain, leading to variations in the band gap, which are then visible as changes in the BE.[25]

In Figure 4d, the difference in the Mo $3d_{5/2}$ peak position before and during gas exposure has been quantified by subtracting the UHV and NO_x maps in Figure 4b,c. This difference map is dominated by a red area in the top-left corner with a homogeneous relative shift in the BE of 0.3 eV, extending far into the channel away from the contacts. Lower changes in the BE are observed in the region close to the drain contact. In this region, the surface is covered by carbon deposited during the initial focused-beam exposure (visible as a dark area of subdued intensity in the maps in Figure S5), possibly preventing gas adsorption and thus causing this area of the channel to be less active in gas sensing.

The small difference in the BE with and without gas along the edge on the right-hand side of the map is less understood. This is the physical edge of the MoS_2 channel, while the left side of the maps in Figure 4 corresponds to the middle of the MoS_2 channel (Figure 4a). We note that inhomogeneities perpendicular to the applied field have been observed in similar devices[24] and could be an edge effect related to nonideal electrical contacts. Given the many sources of local variation in the BE, from inhomogeneous potential distribution to contaminations of various kinds, the analysis of spatial maps is found to be more reliable than individual peak shifts from discrete point measurements.

Figure 4e shows XPS spectra averaged over the channel area indicated by the dotted box in Figure 4b,c. The Mo $3d_{5/2}$ peak maximum is at 230.0 eV in UHV and 229.7 eV in NO_x. A lower BE of the Mo $3d_{5/2}$ state corresponds to a downward shift in the Fermi level (E_F), consistent with NO_x gas making the MoS_2 channel less n-type. To explore the correspondence between the operando SPEM results and the in situ electrical measurements, the shift in E_F was estimated from the transfer characteristics of the device (Figure S3). In UHV, the charge-carrier density (n) was calculated using the parallel-plate capacitor model (eq 1)

$$n = C_t \frac{V_g - V_{th}}{e} \tag{1}$$

where C_t is the total capacitance of the hBN and SiO_2 substrate layers, e is the electron charge, and V_{th} is the threshold voltage. The charge-carrier concentration of $n_{UHV} = 3.43 \times 10^{12}$ cm^{-2} can be translated into a Fermi level position of 23 meV above the conduction-band edge via eq 2

$$E_F = \hbar^2 \pi n / m_e \tag{2}$$

where $m_e = 0.4 m_0$ is the effective electron mass in monolayer MoS_2.[26] In NO_x gas, the current (and thus the charge-carrier concentration) through the device drops to virtually zero (Figure 3), meaning that the corresponding E_F must be inside the band gap of MoS_2. Our transport data do not allow us to quantify the E_F position in NO_x; however, we note that the observed change in the SPEM experiment corresponds well with the energetic position of sulfur vacancies in MoS_2, located 0.2−0.3 eV below the conduction band.[27] In this scenario, sulfur vacancies act as pinning sites, preventing the Fermi level from moving even deeper into the band gap. The changes in the BE observed in Figure 4d are thus qualitatively and quantitatively consistent with charge transfer between MoS_2 and adsorbed NO_x gas species.

Finally, we note that we could not detect an additional component in the Mo $3d_{5/2}$ peak signal, indicative for device oxidation by chemisorbed gas species during several rounds of NO_x dosing and annealing (Section S7). Our experiments show that our devices are fully recoverable by annealing in UHV (Figure S3). It is reasonable to expect that if significant defects are created by the removal of sulfur atoms with the subsequent replacement by oxygen atoms, removal of the oxidant species by UHV annealing should not lead to a full recovery of mobility due to the increased number of vacancies left in the basal plane, which would then act as scattering sites.[28]

However, it is plausible to assume chemisorption of NO_x molecules at preexisting sulfur vacancies. Such a process would have a 2-fold impact on the SPEM results: (i) a reduction in the BE related to a decrease in E_F due to the depletion of charge carriers, as was indeed observed experimentally, and (ii) an additional component in the Mo $3d_{5/2}$ peak signal, reflecting the chemical environment of molybdenum atoms, which we do not observe (Figure 4e). However, reported values for the intrinsic sulfur vacancy concentration in MoS_2 range from 10^{11} to 10^{13} cm^{-2},[29,30] so that even if each sulfur vacancy was decorated with an adsorbed gas molecule, the gas coverage of the MoS_2 surface would only correspond to 10^{-4}−10^{-2} monolayers, which is below the detection limit of this SPEM technique.

In summary, we have performed concurrent operando SPEM and in situ electrical transport measurements to study the interaction of a monolayer MoS_2 gas sensor with NO_x gas molecules. Charge transfer between adsorbed gas species and MoS_2 does indeed result in a less n-type MoS_2 channel. The changes in the BE observed by SPEM are related to electrical transport, and the characteristics of the spatial distribution and gas−solid interaction are discussed. We believe that this study further demonstrates the sensitivity and efficacy of MoS_2 as a gas-sensing nanomaterial.

Materials and Methods. Mechanically exfoliated monolayers MoS_2 were transferred on preprepared 70-nm-thick hBN flakes by a dry transfer technique (Figure S1). The MoS_2 channel was patterned using EBL, followed by reactive ion etching. Finally, electrodes were realized by EBL and electron-beam evaporation and lift-off of titanium/gold (5 nm/110 nm) metals.

The cross-sectional transmission electron microscopy (TEM) sample was prepared by a Helios G4 UX dual-beam focused ion beam−scanning electron microscopy (FIB−SEM) from FEI. A thin layer of gold (≈30 nm thick) was sputter-coated on top of the sample prior to FIB preparation. A 2−3-μm-thick platinum protection layer was deposited on top of the region of interest. The first part of this platinum layer was deposited by electron-beam-assisted deposition to avoid any Ga^+-ion-beam damage to the MoS_2/hBN. The TEM lamella was transferred to a dedicated copper TEM grid by a standard lift-out technique. Coarse thinning was performed with a 30 kV ion-beam acceleration voltage. Final thinning was performed at 5 and 2 kV on either side of the lamella to minimize surface damage. TEM was performed with a JEOL ARM 200F double-cesium aberration-corrected cold field emission gun, operated at 200 kV. The ARM is equipped with a large solid angle (0.98 sr) Centurio detector for energy-dispersive X-ray spectroscopy (EDS) and a GIF Quantum ER for fast dual electron energy loss spectroscopy (EELS).

SPEM was performed at the ESCA microscopy beamline at the Elettra synchrotron in Trieste, Italy. Technical details of the SPEM setup can be found in refs 15 and 16. The X-ray beam energy was 701.3 eV. The maps were acquired using a multichannel delay line detector, which allows one to obtain a small spectrum in the snapshot

https://dx.doi.org/10.1021/acsanm.1c00137
ACS Appl. Nano Mater. 2021, 4, 3319−3324

mode at every pixel of the map and thus allows one to extract the local BE peak position. To extract local BE peak positions, the data were first filtered by applying a 3 × 3 averaging filter to reduce the noise. Using an automated routine, a peak fitting was performed at every pixel. New maps were created containing the obtained peak position for every pixel. To make sure the analysis area is the same with and without gas, the maps in Figure 3 have been adjusted for sample drift (for details, see Figure S5). The effect of beam damage was limited by using a defocused beam and by taking SPEM maps where the beam was rastered across the sample instead of high-energy resolution spectra in a fixed spot (see details in Section S6).

The electrical transport properties of the device were characterized using a two-point configuration with a Keithley 2440 sourcemeter. The gate voltage was applied by a Keithley 2450 instrument, and all data were recorded by a customized *LabVIEW* program.

■ ASSOCIATED CONTENT

Supporting Information

The Supporting Information is available free of charge at https://pubs.acs.org/doi/10.1021/acsanm.1c00137.

Heterostructure assembly process, STEM image of the heterostructure combined with EDS and EELS maps, transfer characteristic curves before and after NO_x exposure, quantitative analysis of the sensor response, SPEM intensity maps, effects of beam damage, and evaluation of molybdenum oxidation (PDF)

■ AUTHOR INFORMATION

Corresponding Authors

Luca Gregoratti − *Elettra Sincrotrone Trieste S.C.p.A., 34149 Trieste, Italy*; Email: luca.gregoratti@elettra.eu

Branson D. Belle − *Department of Sustainable Energy Technology, SINTEF, 0373 Oslo, Norway; Department of Smart Sensor Systems, SINTEF, 0373 Oslo, Norway*; orcid.org/0000-0002-1211-8714; Email: Branson.Belle@sintef.no

Authors

Ingvild J. T. Jensen − *Department of Sustainable Energy Technology, SINTEF, 0373 Oslo, Norway*

Ayaz Ali − *Department of Smart Sensor Systems, SINTEF, 0373 Oslo, Norway; Department of Electronic Engineering, University of Sindh, 76080 Jamshoro, Pakistan*

Patrick Zeller − *Elettra Sincrotrone Trieste S.C.p.A., 34149 Trieste, Italy; Helmholtz-Zentrum Berlin für Materialien and Energie GmbH, BESSY II, 12489 Berlin, Germany; Department of Inorganic Chemistry, Fritz-Haber-Institute of the Max Planck Society, 14195 Berlin, Germany*

Matteo Amati − *Elettra Sincrotrone Trieste S.C.p.A., 34149 Trieste, Italy*

Matthias Schrade − *Department of Sustainable Energy Technology, SINTEF, 0373 Oslo, Norway*

Per Erik Vullum − *Department of Materials and Nanotechnology, SINTEF, 7034 Trondheim, Norway*

Marta Benthem Muñiz − *Institut de Physique de la Matière Complexe, Ecole Polytechnique Fédérale de Lausanne, 1015 Lausanne, Switzerland; Department of Sustainable Energy Technology, SINTEF, 0373 Oslo, Norway*

Prashant Bisht − *Thin Film Laboratory, Department of Physics, Indian Institute of Technology Delhi, 110016 Delhi, India*

Takashi Taniguchi − *International Center for Materials Nanoarchitectonics, National Institute for Materials Science, Tsukuba 305-0044, Japan*; orcid.org/0000-0002-1467-3105

Kenji Watanabe − *Research Center for Functional Materials, National Institute for Materials Science, Tsukuba 305-0044, Japan*; orcid.org/0000-0003-3701-8119

Bodh Raj Mehta − *Thin Film Laboratory, Department of Physics, Indian Institute of Technology Delhi, 110016 Delhi, India*; orcid.org/0000-0002-2888-5897

Complete contact information is available at: https://pubs.acs.org/10.1021/acsanm.1c00137

Author Contributions

I.J.T.J. and B.D.B. conceived the study, T.T. and K.W. prepared materials, and A.A. and B.D.B. fabricated devices. Near-ambient-pressure SPEM investigation and data analysis were carried out by I.J.T.J., B.D.B., A.A., P.Z., M.A., L.G., M.B.M., P.B., B.R.M., and M.S. TEM investigations were carried out by P.E.V. The manuscript was prepared by I.J.T.J., M.S., A.A., and B.D.B. with contributions of all authors.

Notes

The authors declare no competing financial interest.

■ ACKNOWLEDGMENTS

The authors thank D. C. Elias for insightful discussions. This work was supported by the Research Council of Norway (Project 280788). The Research Council of Norway is also acknowledged for support of the Norwegian Micro- and Nano-Fabrication Facility, NorFab (Project 245963/F50), and of the NORTEM infrastructure (Grant 197405), TEM Gemini Centre, Norwegian University of Science and Technology, Trondheim, Norway. K.W. and T.T. acknowledge support from the Elemental Strategy Initiative conducted by the MEXT, Japan (Grant JPMXP0112101001), the JSPS KAKENHI (Grant JP20H00354), and the CREST, JST (Grant JPMJCR15F3).

■ REFERENCES

(1) Lamsal, L. N.; Martin, R. V.; Parrish, D. D.; Krotkov, N. A. Scaling Relationship for NO_2 Pollution and Urban Population Size: A Satellite Perspective. *Environ. Sci. Technol.* **2013**, *47* (14), 7855−7861.

(2) Halliwell, B.; Cross, C. E. Oxygen-derived species: their relation to human disease and environmental stress. *Environ. Health Perspect.* **1994**, *102*, 5−12.

(3) Wetchakun, K.; Samerjai, T.; Tamaekong, N.; Liewhiran, C.; Siriwong, C.; Kruefu, V.; Wisitsoraat, A.; Tuantranont, A.; Phanichphant, S. Semiconducting metal oxides as sensors for environmentally hazardous gases. *Sens. Actuators, B* **2011**, *160* (1), 580−591.

(4) Pham, T.; Li, G.; Bekyarova, E.; Itkis, M. E.; Mulchandani, A. MoS_2-based optoelectronic gas sensor with sub-parts-per-billion limit of NO_2 gas detection. *ACS Nano* **2019**, *13* (3), 3196−3205.

(5) Dontschuk, N.; Stacey, A.; Tadich, A.; Rietwyk, K. J.; Schenk, A.; Edmonds, M. T.; Shimoni, O.; Pakes, C. I.; Prawer, S.; Cervenka, J. A graphene field-effect transistor as a molecule-specific probe of DNA nucleobases. *Nat. Commun.* **2015**, *6* (1), 6563.

(6) Ryou, J.; Kim, Y.-S.; Kc, S.; Cho, K. Monolayer MoS_2 Bandgap Modulation by Dielectric Environments and Tunable Bandgap Transistors. *Sci. Rep.* **2016**, *6* (1), 29184.

(7) Yu, H.; Liao, M.; Zhao, W.; Liu, G.; Zhou, X. J.; Wei, Z.; Xu, X.; Liu, K.; Hu, Z.; Deng, K.; Zhou, S.; Shi, J.-A.; Gu, L.; Shen, C.; Zhang, T.; Du, L.; Xie, L.; Zhu, J.; Chen, W.; Yang, R.; Shi, D.; Zhang, G. Wafer-Scale Growth and Transfer of Highly-Oriented Monolayer MoS_2 Continuous Films. *ACS Nano* **2017**, *11* (12), 12001−12007.

(8) Radisavljevic, B.; Radenovic, A.; Brivio, J.; Giacometti, V.; Kis, A. Single-layer MoS_2 transistors. *Nat. Nanotechnol.* **2011**, *6* (3), 147−150.
(9) Ali, A.; Koybasi, O.; Xing, W.; Wright, D. N.; Varandani, D.; Taniguchi, T.; Watanabe, K.; Mehta, B. R.; Belle, B. D. Single digit parts-per-billion NO_x detection using MoS_2/hBN transistors. *Sens. Actuators, A* **2020**, *315*, 112247.
(10) Dey, S.; Matte, H. S. S. R.; Shirodkar, S. N.; Waghmare, U. V.; Rao, C. N. R. Charge-Transfer Interaction between Few-Layer MoS_2 and Tetrathiafulvalene. *Chem. - Asian J.* **2013**, *8* (8), 1780−1784.
(11) Cho, B.; Hahm, M. G.; Choi, M.; Yoon, J.; Kim, A. R.; Lee, Y.-J.; Park, S.-G.; Kwon, J.-D.; Kim, C. S.; Song, M.; et al. Charge-transfer-based gas sensing using atomic-layer MoS_2. *Sci. Rep.* **2015**, *5*, 8052.
(12) Feng, Y.; Zhang, K.; Li, H.; Wang, F.; Zhou, B.; Fang, M.; Wang, W.; Wei, J.; Wong, H. P. In situ visualization and detection of surface potential variation of mono and multilayer MoS_2 under different humidities using Kelvin probe force microscopy. *Nanotechnology* **2017**, *28* (29), 295705.
(13) Late, D. J.; Huang, Y.-K.; Liu, B.; Acharya, J.; Shirodkar, S. N.; Luo, J.; Yan, A.; Charles, D.; Waghmare, U. V.; Dravid, V. P.; Rao, C. N. R. Sensing Behavior of Atomically Thin-Layered MoS_2 Transistors. *ACS Nano* **2013**, *7* (6), 4879−4891.
(14) Lee, S. Y.; Kim, U. J.; Chung, J.; Nam, H.; Jeong, H. Y.; Han, G. H.; Kim, H.; Oh, H. M.; Lee, H.; Kim, H.; Roh, Y.-G.; Kim, J.; Hwang, S. W.; Park, Y.; Lee, Y. H. Large Work Function Modulation of Monolayer MoS_2 by Ambient Gases. *ACS Nano* **2016**, *10* (6), 6100−6107.
(15) Gregoratti, L.; Al-Hada, M.; Amati, M.; Brescia, R.; Roccella, D.; Sezen, H.; Zeller, P. Spatially Resolved Photoelectron Spectroscopy from Ultra-high Vacuum to Near Ambient Pressure Sample Environments. *Top. Catal.* **2018**, *61* (12), 1274−1282.
(16) Zeller, P.; Amati, M.; Sezen, H.; Scardamaglia, M.; Struzzi, C.; Bittencourt, C.; Lantz, G.; Hajlaoui, M.; Papalazarou, E.; Marino, M.; Fanetti, M.; Ambrosini, S.; Rubini, S.; Gregoratti, L. Scanning Photoelectron Spectro-Microscopy: A Modern Tool for the Study of Materials at the Nanoscale. *Phys. Status Solidi A* **2018**, *215* (19), 1800308.
(17) Castellanos-Gomez, A.; Buscema, M.; Molenaar, R.; Singh, V.; Janssen, L.; Van Der Zant, H. S.; Steele, G. A. Deterministic transfer of two-dimensional materials by all-dry viscoelastic stamping. *2D Mater.* **2014**, *1* (1), 011002.
(18) Li, H.; Yin, Z.; He, Q.; Li, H.; Huang, X.; Lu, G.; Fam, D. W. H.; Tok, A. I. Y.; Zhang, Q.; Zhang, H. Fabrication of Single- and Multilayer MoS_2 Film-Based Field-Effect Transistors for Sensing NO at Room Temperature. *Small* **2012**, *8* (1), 63−67.
(19) Nan, H.; Wang, Z.; Wang, W.; Liang, Z.; Lu, Y.; Chen, Q.; He, D.; Tan, P.; Miao, F.; Wang, X.; Wang, J.; Ni, Z. Strong Photoluminescence Enhancement of MoS_2 through Defect Engineering and Oxygen Bonding. *ACS Nano* **2014**, *8* (6), 5738−5745.
(20) Kang, Y.; Pyo, S.; Jo, E.; Kim, J. Light-assisted recovery of reacted MoS_2 for reversible NO_2 sensing at room temperature. *Nanotechnology* **2019**, *30* (35), 355504.
(21) Yue, Q.; Shao, Z.; Chang, S.; Li, J. Adsorption of gas molecules on monolayer MoS_2 and effect of applied electric field. *Nanoscale Res. Lett.* **2013**, *8* (1), 425.
(22) Sun, L.; Zhang, X.; Liu, F.; Shen, Y.; Fan, X.; Zheng, S.; Thong, J. T.; Liu, Z.; Yang, S. A.; Yang, H. Y. Vacuum level dependent photoluminescence in chemical vapor deposition-grown monolayer MoS_2. *Sci. Rep.* **2017**, *7* (1), 1−9.
(23) Vaknin, Y.; Dagan, R.; Rosenwaks, Y. Pinch-Off Formation in Monolayer and Multilayers MoS_2 Field-Effect Transistors. *Nanomaterials* **2019**, *9* (6), 882.
(24) Yi, Y.; Wu, C.; Liu, H.; Zeng, J.; He, H.; Wang, J. A study of lateral Schottky contacts in WSe_2 and MoS_2 field effect transistors using scanning photocurrent microscopy. *Nanoscale* **2015**, *7* (38), 15711−15718.
(25) Kretinin, A. V.; Cao, Y.; Tu, J. S.; Yu, G. L.; Jalil, R.; Novoselov, K. S.; Haigh, S. J.; Gholinia, A.; Mishchenko, A.; Lozada, M.; Georgiou, T.; Woods, C. R.; Withers, F.; Blake, P.; Eda, G.; Wirsig, A.; Hucho, C.; Watanabe, K.; Taniguchi, T.; Geim, A. K.; Gorbachev, R. V. Electronic Properties of Graphene Encapsulated with Different Two-Dimensional Atomic Crystals. *Nano Lett.* **2014**, *14* (6), 3270−3276.
(26) Cheiwchanchamnangij, T.; Lambrecht, W. R. L. Quasiparticle band structure calculation of monolayer, bilayer, and bulk MoS_2. *Phys. Rev. B: Condens. Matter Mater. Phys.* **2012**, *85* (20), 205302.
(27) Fabbri, F.; Rotunno, E.; Cinquanta, E.; Campi, D.; Bonnini, E.; Kaplan, D.; Lazzarini, L.; Bernasconi, M.; Ferrari, C.; Longo, M.; Nicotra, G.; Molle, A.; Swaminathan, V.; Salviati, G. Novel near-infrared emission from crystal defects in MoS_2 multilayer flakes. *Nat. Commun.* **2016**, *7* (1), 13044.
(28) Yanase, T.; Uehara, F.; Naito, I.; Nagahama, T.; Shimada, T. Healing Sulfur Vacancies in Monolayer MoS_2 by High-Pressure Sulfur and Selenium Annealing: Implication for High-Performance Transistors. *ACS Applied Nano Materials* **2020**, *3* (10), 10462−10469.
(29) Qiu, H.; Xu, T.; Wang, Z.; Ren, W.; Nan, H.; Ni, Z.; Chen, Q.; Yuan, S.; Miao, F.; Song, F.; Long, G.; Shi, Y.; Sun, L.; Wang, J.; Wang, X. Hopping transport through defect-induced localized states in molybdenum disulphide. *Nat. Commun.* **2013**, *4* (1), 2642.
(30) Pető, J.; Ollár, T.; Vancsó, P.; Popov, Z. I.; Magda, G. Z.; Dobrik, G.; Hwang, C.; Sorokin, P. B.; Tapasztó, L. Spontaneous doping of the basal plane of MoS_2 single layers through oxygen substitution under ambient conditions. *Nat. Chem.* **2018**, *10* (12), 1246−1251.

https://dx.doi.org/10.1021/acsanm.1c00137
ACS Appl. Nano Mater. 2021, 4, 3319−3324